Liu *et al. Sustainable Environment Research* (2024) 34:27
https://doi.org/10.1186/s42834-024-00233-x

Sustainable Environment Research

RESEARCH Open Access

Biosorption of Pb^{2+}, Cd^{2+} and Zn^{2+} from aqueous solutions by *Agrobacterium tumefaciens* S12 isolated from acid mine drainage

Shuli Liu[1,2], Xiaojun Xu[2], Changhua He[1], Zhangyang Liu[1] and Yan Li[1*]

Abstract

Heavy metal pollution is a global environmental issue, and microorganisms play a crucial role in the bioremediation of heavy metal-contaminated wastewater. The study isolated heavy metal-resistant bacterium and observed their absorption ability toward Pb^{2+}, Cd^{2+} and Zn^{2+}. We isolated *Agrobacterium tumefaciens* S12 from acid mine drainage. The various factors influencing its adsorption performance, including pH, biomass dosage, initial metal ion concentration, and adsorption temperature, were investigated in detail. Chemisorption controls the adsorption rate due to the results better fitted by pseudo-second order kinetics. The maximum adsorption capacities of Pb^{2+}, Cd^{2+} and Zn^{2+} on *A. tumefaciens* S12 were 234, 58 and 51 mg g^{-1} at 30 °C from Langmuir isotherm, respectively. The adsorption processes for the three heavy metal ions were spontaneous and exothermic in nature. In bimetallic systems, biosorption of Pb^{2+} ions was preferential to that of Cd^{2+} and Zn^{2+}. Furthermore, scanning electron microscopy coupled to energy dispersive spectroscopy, Fourier-transform infrared spectra and X-ray photoelectron spectroscopy analysis demonstrated that the adsorption mechanisms include ion-exchange, complexation interaction between the heavy metal ions and the functional groups on the surface of biomass. The obtained results indicated that *A. tumefaciens* S12 can be applied as an efficient biosorbent in bioremediation technology to sequestrate heavy metal ions from aqueous solution.

Keywords Acid mine drainage, *Agrobacterium tumefaciens*, Biosorbent, Heavy metal, Biosorption

1 Introduction

The metal productions are main processes from the industries of mining, mineral processing and extractive metallurgy, and these industrial activities may cause environmental pollution [1, 2]. Acid mine drainage (AMD) comes from non-valuable sulfide minerals reacting with water and oxygen [3]. ADM possesses the features of low pH containing large amount of hazardous heavy metals and metalloids [4–6]. Heavy metals tend to accumulate in living organisms as they are not biodegradable that can cause ecological pollution and pose a threat to human health. Various traditional physicochemical methods including chemical precipitation, ion exchange resins, membrane filtration, electrodialysis, coagulation and flocculation have already been exploited to treat wastewater containing heavy metal [7, 8]. Each method has its own merits and drawbacks for removal of heavy metals from wastewater [9–11]. For example, chemical precipitation is easy to operate and cost-effective for treatment

*Correspondence:
Yan Li
liyan067321@sina.com
[1] School of Public Health, Zunyi Medical University, Zunyi 563003, China
[2] Faculty of Environmental Science and Engineering, Kunming University of Science and Technology, Kunming 650500, China

of heavy metals. Nevertheless, it has the following disadvantages, such as producing a large amount of sludge, increasing cost for sludge disposal, and having low efficiency for low heavy metal concentration [12]. Whilst ion exchange resins own the advantages of high removal efficiency and short processing periods, it is high cost for the synthesis of resin and can cause secondary pollution due to regeneration of the resins. For membrane filtration, it possesses the merits of high selectivity, small area occupancy and low-pressure requirement with these drawbacks containing high operational cost, complicated operation and low flux limiting its application [13]. Electrodialysis with high selectivity requires high cost because of energy consumption and membrane fouling. Although the process of coagulation and flocculation has the ability of removing multiple pollutants, it can generate sludge and is ineffective for heavy metals removal without combination with other treatment techniques.

Biosorption is one method of bioremediation, and it can be defined as the passive uptake of pollutants by using bio-derived products or waste materials as biosorbents to separate heavy metals from aqueous solutions [7]. Bioadsorption has gained enormous attention for its superiority in many aspects. Compared with traditional methods, bioadsorption is easy to conduct, environment-friendly, low cost and low energy-consumption. Additionally, bioadsorption can effectively remove soluble and insoluble pollutants without generating hazardous by-products [14]. Bioadsorption is effective when treating low metal concentration drinking water and can be regenerated for circle reuse [15]. Biosorption is dependent on active substances owing to the ability of metal- binding on surface of biomass [16]. The surface of microbes containing bacteria, fungi and algae has many functional groups, for instance, carboxyl, phosphate, hydroxyl or amine provided by polysaccharide, protein and lipid with the adsorption capability for the removal of heavy metal ions [17–19]. Living and dead microbial cells as biological adsorbent have been extensively studied [20]. Living microorganisms can be used to investigate tolerance to heavy metals and adsorption specificity to different heavy metals [21]. Resistance mechanisms of microorganisms to some harmful heavy metals have been developed and therefore these special microorganisms are potential biological materials to remediate wastewater containing heavy metals [22–24].

Therefore, finding microorganisms with heavy metal resistance for environmental remediation is a key process for biosorption technology. In addition, for biosorption use in the remediation of heavy metals, the source, safety, cost, and adsorption capacity should be considered for the selection of any suitable biomaterial. *Agrobacterium tumefaciens* are Gram-negative bacterium, generally exists on the root surface of plants and lives on nutrients infiltrated from root tissues [25]. It shows better biosecurity based on its wide application in plant genetic engineering [26, 27]. Easy and cheap preparation of *A. tumefaciens* lowers its application cost and makes it competitive among various bio-sorbents. Besides, simultaneous removal of multiple metal ions from complex environments using bioadsorption remains a challenge. Herein, we studied the *A. tumefaciens* with heavy metal resistant isolated from AMD, then explored in detail its adsorption performance in single and bimetallic systems, isothermal behavior and adsorption kinetics for Pb^{2+}, Cd^{2+} and Zn^{2+}. Subsequently, the scanning electron microscopy coupled to energy dispersive spectroscopy (SEM), Fourier-transform infrared spectra (FTIR) and X-ray photoelectron spectroscopy (XPS) characterization were carried out to clarify adsorption mechanisms of *A. tumefaciens* S12.

2 Materials and methods

2.1 Materials

This study used analytic grade chemical reagents to conduct all experiments. These chemicals included beef extract, peptone (Beijing Aoboxing Biotechnology Co., China), yeast extract (Shanghai Swan Beer Co., China), glucose (Tianjin Shengao Chemical Reagent Co., China), NaCl, $Pb(NO_3)_2$ (Tianjin Fengchuan Chemical Reagent Technology Co., China), $Cd(NO_3)_2$ (Tianjin Damao Chemical Reagent Factory, China) and $Zn(NO_3)_2$ (Chengdu Kelong Chemical Reagent factory, China). All reagents were prepared with ultrapure water (GWB-1E/2E water purification system, Beijing General Instrument Co., China).

2.2 Sampling sites and isolation of bacterial strains

The used bacteria in this study were isolated from AMD with pH value of 6.12 in the Yunnan province, China in 2015. In this study, five AMD samples were collected, with the average levels of Pb, Cd, and Zn in these samples being 0.43, 0.015, and 1.12 mg L^{-1}, respectively. An atomic absorption spectrophotometer (AAS, TAS-990AFG, China) was used to analyze the concentration of metal ions in the sample. Water sample was collected and stored in sterile glass bottle. Dilution technique was applied to isolate microorganisms from obtained water samples [21]. Fully mix with vortex 10 mL water sample and sterilized 90 mL water to attain 10^{-1} dilute solution. We applied 100 µL of 10^{-4}–10^{-6} dilute solution spreading on Nutrient Agar (NA) and incubated at a constant temperature incubator (MJPS-150, China) for 3–5 d at 30 ℃. After incubation periods, strains were purified through repeated plate streaking. The purified isolates were observed under light microscopy.

2.3 Minimum inhibitory concentrations (MIC) of Pb^{2+}, Cd^{2+} and Zn^{2+}

MIC represents the minimum heavy metal concentrations at which the strains cannot grow normally. We used $Pb(NO_3)_2$, $Cd(NO_3)_2$ and $Zn(NO_3)_2$ as source of metal ions to conduct our experiments. The heavy metal ions solutions were added to sterilized and cooled NA (about 50 ℃). The number of microbial cells in each culture flask is approximate 1.5×10^5 CFU mL^{-1} and culture temperature is 30 ℃. After 2 d, aliquots of 100 μL bacterial suspension was spread onto NA and observed visually the growth of strains regularly. The concentration of Pb^{2+}, Cd^{2+} and Zn^{2+} in the nutrient broth was gradually increased while keeping other conditions unchanged until no bacteria grew on the NA. Tolerance of isolates to heavy metal was determined by comparing MIC values of isolates obtained from this study and *Bacillus subtilis* NRRL-B-209 strain [28]. Among the isolated bacteria, three strains, designated as S1, S5, and S12, demonstrated superior resistance to Pb^{2+}, Cd^{2+}, and Zn^{2+} at a concentration of 250 mg L^{-1} compared to other strains. Therefore, they were selected for further confirmation through morphological and molecular characterization.

2.4 Identification of *bacteria*

Gram stain was used for determining G(+) or G(-) of the three strains. 16S rDNA sequencing was utilized to analyze molecular characterization of isolated bacteria. Extracting total DNA with Ezup column bacterial genomic DNA extraction kit (Sangon Biotech, China.) was the first step, and then 16S rDNA was amplified using bacterial universal primers. The amplification was performed in a specific mixture involving 0.5 μL template, 2.5 μL 10 X PCR buffer, 1 μL dNTP (2.5 mM), 0.2 μL Tap polymerase, 0.5 μL F(10 μM), 0.5 μL R(10 uM) and then added distilled water to 25 μL. The procedure of PCR reaction was conducted following these steps: the first step is denaturation for 4 min under 94 ℃, then performing 30 times denaturation (94 ℃, 45 s) followed by annealing (55 ℃, 45 s) and extension (72 ℃, 1 min). After finishing above steps, it needs to repair extension for 10 min and control the temperature at 72 ℃. Finally, the reaction was terminated at 4 ℃. The electrophoresis was used to extract the amplified fragments through 1.0% agarose gels, which was treated for 20 min under 150 V. Molecular weight marker can be completed by using specific DNA ladder ranging from100 bp to 10 kb. Sequencing of obtained gel purified amplicon was completed by Sangon Biotech (Shanghai), China. Obtaining DNA sequences were imported onto the web of National Center for Biotechnology Information to compare with reference strains. The phylogenetic tree of isolated strains was made by Clustal X 1.83 software and MEGA version 7.0.

2.5 Bacterial preparation as a biosorbent

The strain S12 was identified as *A. tumefaciens*, exhibiting a higher adsorption capacity than the other strains. Therefore, it was selected as biosorbent for removing heavy metals in wastewater. This strain S12 was cultivated in 250 mL volumetric flasks including 100 mL nutrient broth. Biosorbent used subsequently was prepared through the following steps: collecting bacterial cells through centrifugation (10,000 rpm, 4 ℃) by a centrifuge (GL-21 M, China) at late-exponential stage cultivating (28 ± 2 ℃, 150 rpm) in an incubator (SPH-1112D, China), and then washing these cells 3 times using deionized water that had been sterilized. Harvested cells from the last step were stored in refrigerator with 4 ℃ after centrifuging [29].

2.6 Batch biosorption studies

In single systems, various influencing factors were considered, including pH, S12 dosage, concentrations of heavy metal ions added to the reactor, adsorption time and temperatures. A certain amount of heavy metal solution with different concentrations and *A. tumefaciens* S12 (dry weight) were placed in conical flasks to measure the pH, which were cultivated in a rotary shaker with setting specified time, temperature and rotate speed. The mixtures were obtained by centrifuging about 10 min under the conditions of 10,000 rpm, 4 ℃ after the absorption process reached equilibrium. Then the supernatant was used to analyze residual concentration of studied metal ions through AAS. For this study, each experiment was repeated 3 times, and experimental results were analyzed using the average values.

R (%) and q_e (mg g^{-1}) were used to display the removal efficiency and adsorption capacity of S12 for heavy metal ions, respectively. They were obtained through Eqs. (1) and (2), respectively.

$$R = \frac{C_0 - C_e}{C_0} \times 100\% \tag{1}$$

$$q_e = \frac{(C_0 - C_e) \times V}{m} \tag{2}$$

where C_0 and C_e are the initial and equilibrium concentrations of heavy metal ions (mg L^{-1}), respectively. V (L) and m (g) are reaction volume and amount of biosorbent, respectively.

For bimetallic systems (Cd /Pb, Zn/ Pb and Cd/Zn), initial Pb^{2+}, Cd^{2+} and Zn^{2+} concentrations were regulated from 0 to 100 mg L^{-1}. Changing another metal ion concentration in above bimetallic systems was done when the concentration of the first metal ion was fixed.

2.7 Characterization analysis

The dried S12 biosorbent (free and metal treated) was obtained about 48 h through vacuum freeze drying oven at -50 ℃. The SEM–EDS (JSM-7500F, Japan) showed the morphology characteristics and elemental distribution of the tested samples at 20 kV acceleration voltage. The FTIR was conducted by a Perkin Elmer spectrometer (Nicolet iS5N, USA), using KBr as one of the materials and controlling the mass ratio of KBr to tested sample as 700/1. XPS was also used to further illustrate the surface element situation of the samples by Kratos Axis Ultra DLD (Escalab 250Xi, USA) and room temperature could meet temperature requirements of this test. Al Kα X-rays (hν = 1486.6 eV) could provide monochromatic beam to obtain ejected photoelectrons, and the binding energy of the elemental peaks obtained from tested samples is based on the C1s peak.

3 Results and discussion

3.1 Isolation and heavy metal resistances of microorganisms

Forty-five bacterial strains were isolated from AMD, and their resistance to Pb^{2+}, Cd^{2+} and Zn^{2+} was studied. The results indicated that eight strains exhibited stronger resistance to these heavy metal ions compared to the others (Fig. 1). The MIC of three isolates (designated as S1, S5, and S12) for Pb^{2+}, Cd^{2+} and Zn^{2+} exceeded 250 mg L^{-1}, demonstrating higher resistance than other strains. Consequently, these strains were selected for further identification through morphological and molecular characterization.

3.2 Phenotypic and genotypic characterizations

Three heavy-metal-resistant S1, S5 and S12 were identified as *Klebsiella sp.*, *Bacillus megaterium* and *A. tumefaciens*. The isolated *A. tumefaciens* exhibited a higher adsorption capacity than strains S1 and S5, making it the primary focus of this study. Gram staining (Fig. 2) revealed that strain S12 is a Gram-negative, rod-shaped bacterium.

The identity of S12 was further confirmed through 16S rDNA sequencing. A comparison of the 16S rDNA

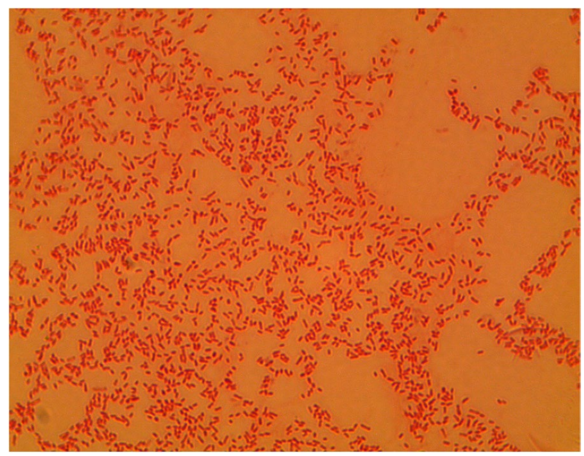

Fig. 2 Gram staining of S12 strain

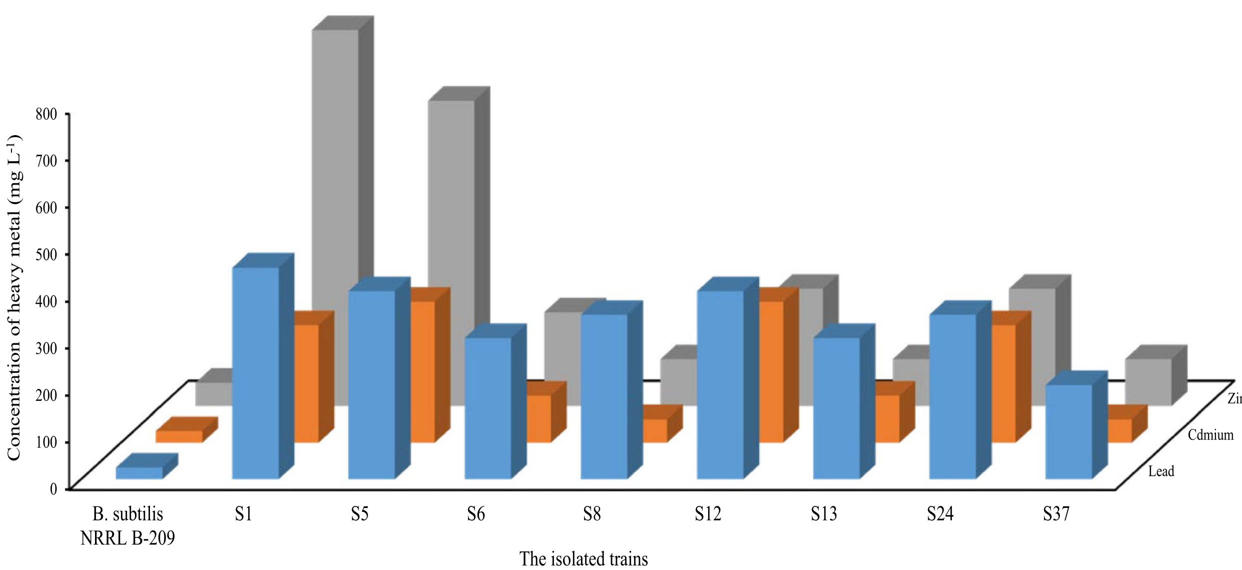

Fig. 1 The resistance of isolated strains towards Pb^{2+}, Cd^{2+} and Zn^{2+}

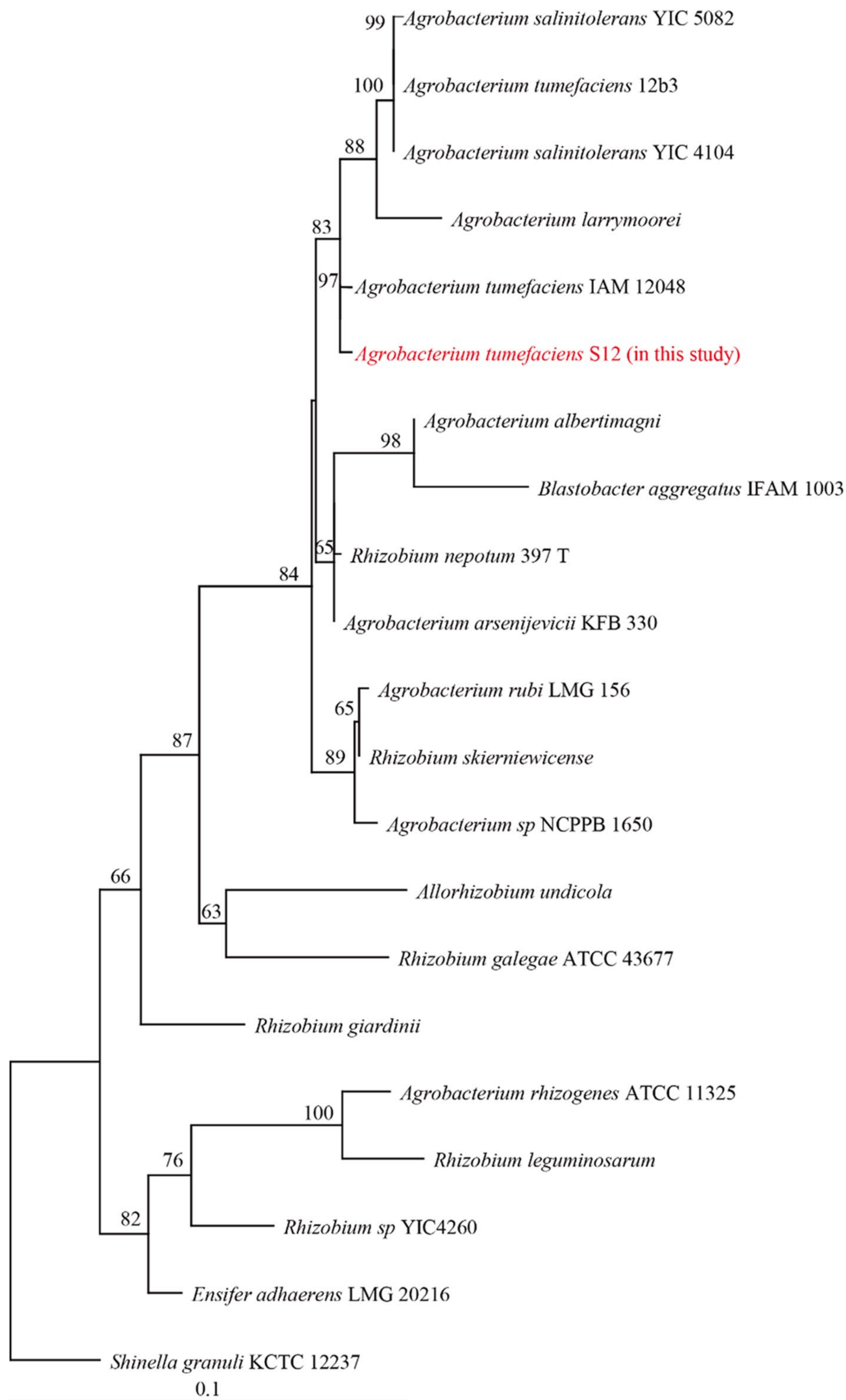

Fig. 3 Phylogenetic tree of S12

sequence between S12 and known sequences indicated that it belongs to the *Agrobacterium* or *Rhizobium genera*, with 100% similarity to *A. tumefaciens*. Additionally, Fig. 3 presents a phylogenetic tree illustrating the evolutionary relationships between S12 and its closest bacterial relatives. These findings confirm that S12 can be identified as *A. tumefaciens*. This strain was subsequently used as a biosorbent to remove Pb^{2+}, Cd^{2+}, and Zn^{2+} from wastewater.

3.3 Batch biosorption studies

3.3.1 Effect of pH

Adsorption properties influenced by pH were assessed through experiments conducted at various pH levels. Within the pH range of 2.0 to 5.5, the adsorption capacity of *A. tumefaciens* S12 for Pb^{2+}, Cd^{2+}, and Zn^{2+} increased correspondingly, likely due to the deprotonation of functional groups [30]. The experimental results indicated that the maximum adsorption capacities for Pb^{2+}, Cd^{2+}, and Zn^{2+} were 182, 53, and 31 mg g^{-1}, respectively, at an optimal pH of 5.5 (Fig. 4a). A slight decrease in adsorption capacities was observed when the pH exceeded 5.5, possibly due to the formation of hydroxide precipitates, which could interfere with the adsorption process [31, 32]. Zeta potential measurements were performed to determine the optimal pH range for metal sorption. The Zeta potential represents the point where the sorbent surface charge is neutralized, known as the point of zero charge (pHzpc). When the pH is below the pHzpc, the adsorbent carries a positive charge, leading to electrostatic repulsion with metal ions and inhibiting adsorption. Conversely, at pH levels above the pHzpc, the adsorbent acquires a negative charge, enhancing its adsorption ability. The pHzpc value for *A. tumefaciens* S12 was estimated to be 3.25, indicating that metal sorption is favored at pH levels higher than 3.25. Consequently, a pH of 5.5 was selected for subsequent experiments, as this value promotes the dissociation of functional groups, enhancing metal ion adsorption while minimizing hydroxide precipitation.

3.3.2 Effect of biomass dosage

Figure 5 shows that the concentration of *A. tumefaciens* S12 had a significant impact on the adsorption of heavy metal ions. Increasing the concentration of *A. tumefaciens* S12 enhanced the removal of Pb^{2+}, Cd^{2+}, and Zn^{2+}, likely due to the increased availability of functional groups for metal ion binding as the adsorbent dosage increased. The removal efficiency (R value) of Pb^{2+} notably increased from 34 to 73% as the biomass dosage was raised from 0.01 g to 0.02 g (dry weight). Similarly, the removal efficiencies of Cd^{2+} and Zn^{2+} improved from 9% and 1.0% to 51% and 40%, respectively, when the biomass dosage was increased from 0.01 g to 0.05 g. However, when the concentration of *A. tumefaciens* S12 exceeded certain thresholds (Pb^{2+}, 0.02 g; Cd^{2+} and Zn^{2+}, 0.05 g), no significant further improvement in the removal rate was observed. Consequently, dosages of 0.02 g, 0.05 g, and 0.05 g of *A. tumefaciens* S12 were selected for follow-up research on the removal of Pb^{2+}, Cd^{2+}, and Zn^{2+}, respectively.

3.3.3 Adsorption kinetics

Figure 6 illustrates the impact of reaction time on the adsorption capacity of *A. tumefaciens* S12 for Pb^{2+}, Cd^{2+}, and Zn^{2+}. According to the experimental results shown in Fig. 6, the adsorption process can be roughly divided into three stages, reaching equilibrium within 60 min. The rapid uptake phase, designated as the first stage, occurs within the first 30 min, during which the

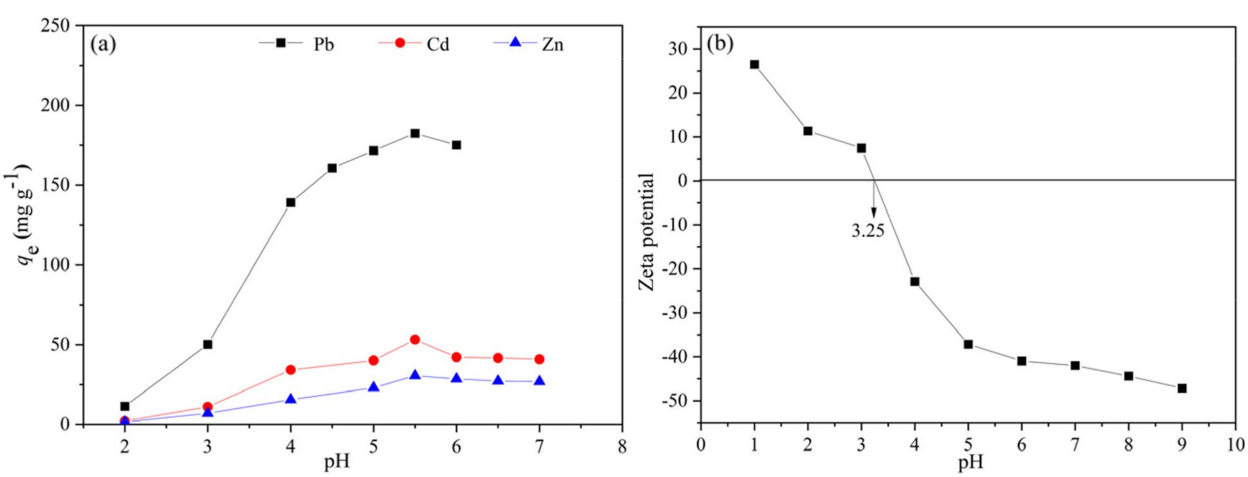

Fig. 4 Effect of pH on the adsorption of Pb^{2+} (**a**), Cd^{2+} and Zn^{2+} by *A. tumefaciens* S12 and Zeta potential of *A. tumefaciens* S12 (**b**)

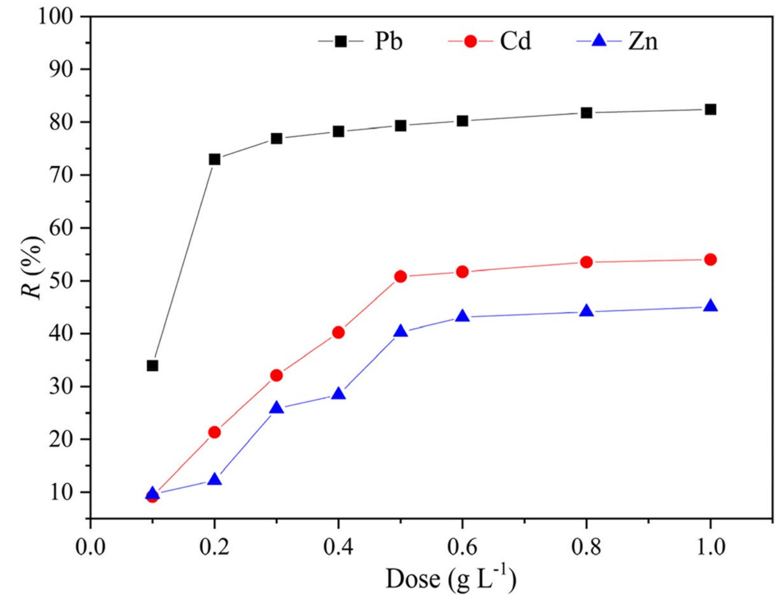

Fig. 5 Effect of biosorbent dosage on the adsorption of Pb^{2+}, Cd^{2+} and Zn^{2+} by *A. tumefaciens* S12

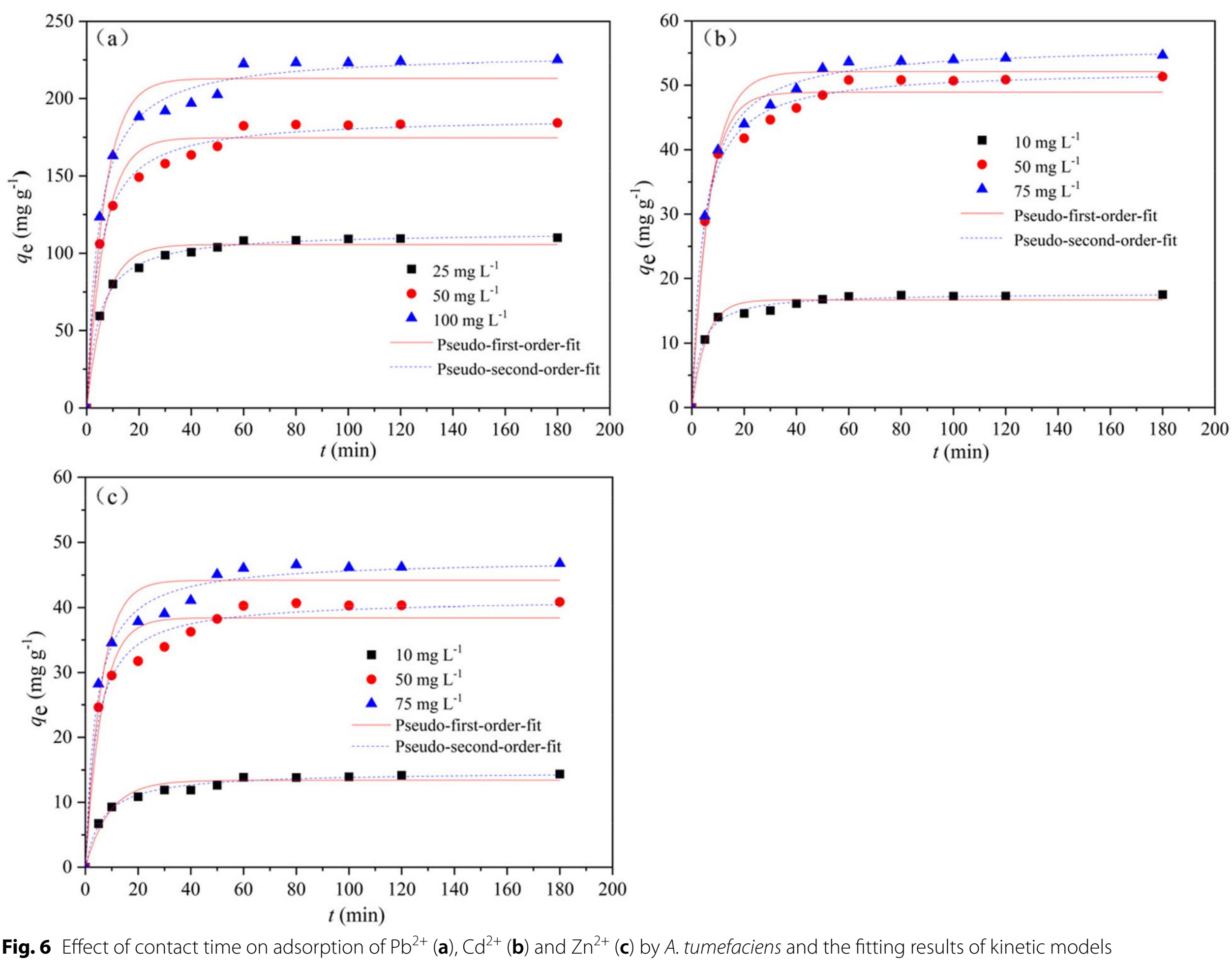

Fig. 6 Effect of contact time on adsorption of Pb^{2+} (**a**), Cd^{2+} (**b**) and Zn^{2+} (**c**) by *A. tumefaciens* and the fitting results of kinetic models

adsorption capacity increases significantly with time. In this initial stage, the adsorbent provides numerous available active sites, and mass transfer resistance is minimal [28]. Additionally, this adsorption process may be spontaneous and does not require energy consumption. The subsequent stage is characterized by slower adsorption. In the later period of adsorption, adsorption capacity appeared slight drop caused by insufficient active sites and difficulty in occupying empty sites. This is caused by repulsive forces between heavy metal ions in the solid and liquid phases [33]. Finally, the active sites become saturated with adsorbed heavy metal ions, and the adsorption process reaches equilibrium at 60 min. To further analyze the adsorption kinetics, two typical models, the pseudo-first-order (Eq. (3)) and pseudo-second-order (Eq. (4)), were applied to the experimental data.

$$q_t = q_e\left(1 - e^{-k_1 t}\right) \tag{3}$$

$$q_t = \frac{k_2 q_e^2 t}{1 + k_2 q_e t} \tag{4}$$

where qt represents the adsorption amount at time t (min) in mg g^{-1}, and k_1 (min^{-1}) and k_2 (g mg^{-1} min^{-1}) are the rate constants for the respective models. Figure 6 and Table 1 show the fitting results.

The correlation coefficients (r^2) in Table 1 fitting from Eq. (4) are better than Eq. (3). Moreover, the q_e values obtained from Eq. (4) at various heavy metal ions concentrations align more closely with the experimental values compared to those from Eq. (3). Luo et al. [34] proposed that the pseudo-second-order model effectively explains dynamic data. This classic model suggests that chemisorption controls the adsorption rate and predicts the entire adsorption process based on the sorption capacity of the sorbent.

3.3.4 Isothermal study

Figure 7a illustrates how the initial concentrations of Pb^{2+}, Cd^{2+}, and Zn^{2+} affect the adsorption capacity of *A. tumefaciens* S12. The change of adsorption capacity was consistent with the change of initial Pb^{2+}, Cd^{2+} and Zn^{2+} concentration. This can be attributed to the increased collision frequency between *A. tumefaciens* S12 and the heavy metal ions as the concentration of metal ions increases in the solution. Higher Pb^{2+}, Cd^{2+} and Zn^{2+} concentration leads to a corresponding increase in adsorption capacity, as the higher concentration gradient effectively reduces mass transfer resistance, allowing more ions to reach the surface of *A. tumefaciens* S12 [35]. The q_e remained nearly unchanged when the initial heavy metal ions concentrations exceeded certain value (the initial Pb^{2+}, Cd^{2+} and Zn^{2+} concentration were 100, 50 and 50 mg L^{-1}, respectively, in this work) because of the saturation of active sites on *A. tumefaciens* S12.

Two representative isotherm models, the Langmuir (Eq. (5)) and Freundlich (Eq. (6)) isotherm models, were applied to further fit the experimental data, as shown in Fig. 7b.

$$q_e = \frac{\mathrm{q_m K_L C_e}}{1 + \mathrm{K_L C_e}} \tag{5}$$

$$q_e = \mathrm{K}_F C_e^{1/n} \tag{6}$$

where q_m (mg g^{-1}) and K_L (L mg^{-1}) from Eq. (5) represent the fitted maximum adsorption capacity and the Langmuir model constant, respectively, for the adsorption process of *A. tumefaciens* S12 for heavy metal ions. K_F [(mg g^{-1}) (L mg^{-1})$^{1/n}$] and $1/n$ from Eq. (6) describe Freundlich model constant and the empirical parameter. The reaction intensity between heavy metal ions and *A. tumefaciens* S12 affects K_F, and $1/n$ can vary according to the adsorption intensity.

Table 1 Adsorption kinetic parameters of *A. tumefaciens* S12 for Pb^{2+}, Cd^{2+} and Zn^{2+}

Metal ions	C_0 (mg L^{-1})	$q_{e,exp}$ (mg g^{-1})	Pseudo-first-order			Pseudo-second-order		
			k_1	q_e (mg g^{-1})	r^2	k_2	q_e (mg g^{-1})	r^2
Pb^{2+}	25	108	0.14	106	0.9778	0.0019	114	0.9982
	50	182	0.15	175	0.9561	0.0012	188	0.9916
	100	222	0.15	213	0.9622	0.0009	230	0.9911
Cd^{2+}	10	17	0.18	17	0.9671	0.0166	18	0.9910
	50	50	0.16	49	0.9675	0.0047	52	0.9932
	75	53	0.14	52	0.9676	0.0039	56	0.9948
Zn^{2+}	10	13	0.11	13	0.9549	0.0106	15	0.9911
	50	40	0.16	38	0.9389	0.0059	41	0.9833
	75	46	0.17	44	0.9479	0.0054	47	0.9859

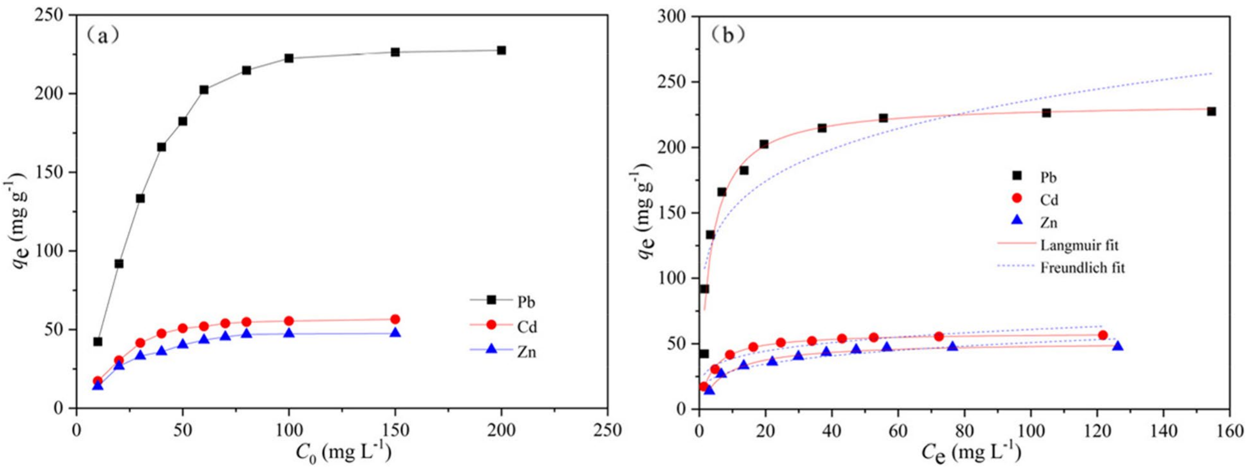

Fig. 7 Effect of initial Pb^{2+}, Cd^{2+} and Zn^{2+} concentration (**a**) and isotherms curve (**b**)

Table 2 Fitting results of experimental data through two isotherms models

Metal ions	$q_{e,exp}$ (mg g^{-1})	Langmuir model			Freundlich model		
		q_{max} (mg g^{-1})	K_L	r^2	K_F	n	r^2
Pb^{2+}	222	234	0.31	0.9504	99	5.3	0.7547
Cd^{2+}	55	58	0.26	0.9940	25	5.1	0.8426
Zn^{2+}	47	51	0.14	0.9805	17	4.2	0.8570

The results fitted by these two models and displayed in Fig. 7b and Table 2 illustrate the Eq. (5) provides a better fit than Eq. (6), based on the correlation coefficient (r^2) and q_m values. This suggests that the surface of *A. tumefaciens* S12 is homogenous, and the adsorption process follows monolayer adsorption. The K_L values for the adsorption of Pb^{2+}, Cd^{2+} and Zn^{2+} were 0.31, 0.26 and 0.14 L mg^{-1}, respectively, indicating that the affinity between heavy metals ions and *A. tumefaciens* S12 follows the order: $Pb^{2+} > Cd^{2+} > Zn^{2+}$. Additionally, the n values between 1 and 10 suggest that *A. tumefaciens* S12 is a favorable adsorbent for the removal of Pb^{2+}, Cd^{2+} and Zn^{2+}.

The q_m values for Pb^{2+}, Cd^{2+} and Zn^{2+} determined by Langmuir isotherm are compared with those reported in the literature, as shown in Table 3. This comparison indicates that *A. tumefaciens* S12 has significant potential for adsorbing heavy metal ions, particularly Pb^{2+}.

Table 3 Comparison of biosorption capacities of *A. tumefaciens* S12 for Pb^{2+}, Cd^{2+} and Zn^{2+} with other biosorbents

Biosorbents	Maximum metal adsorption capacity (mg g^{-1})			References
	Pb^{2+}	Cd^{2+}	Zn^{2+}	
A. tumefaciens	234	58	51	This study
Pseudomonas putida	76	-	-	[36]
Pectobacterium sp. ND2	31	45	34	[31]
Arthrobacter sp. GQ-9	18	-	-	[37]
Bacillus pumilus sp. AS1	134	-	-	[38]
Geobacillus thermoleovorans sub.sp. stromboliensis	-	39	29	[39]
Bacillus catenulatus JB-022 atrain	-	64	-	[40]
Pseudomonas aeruginosa B237	-	17	-	[30]
Tsukamurell apaurometabola A155	-	-	17	[30]
Bacillus cereus AUMC B52	-	-	67	[41]
Klebsiella sp. 3S1	-	-	48	[42]

3.3.5 Thermodynamic study

Temperature is an important influencing factor for adsorption process and was investigated. Figure 8a presents the results. As the temperature increased, the q_e values for Pb^{2+} initially rose, reaching a maximum at 30 °C, before subsequently decreasing. The increase in temperature enhances the kinetic energy of metal ions and increases their collision frequency with the adsorbent, leading to higher adsorption capacity [35]. However, excessive temperature (35 ℃ in this study) can damage binding bonds, resulting in a decrease

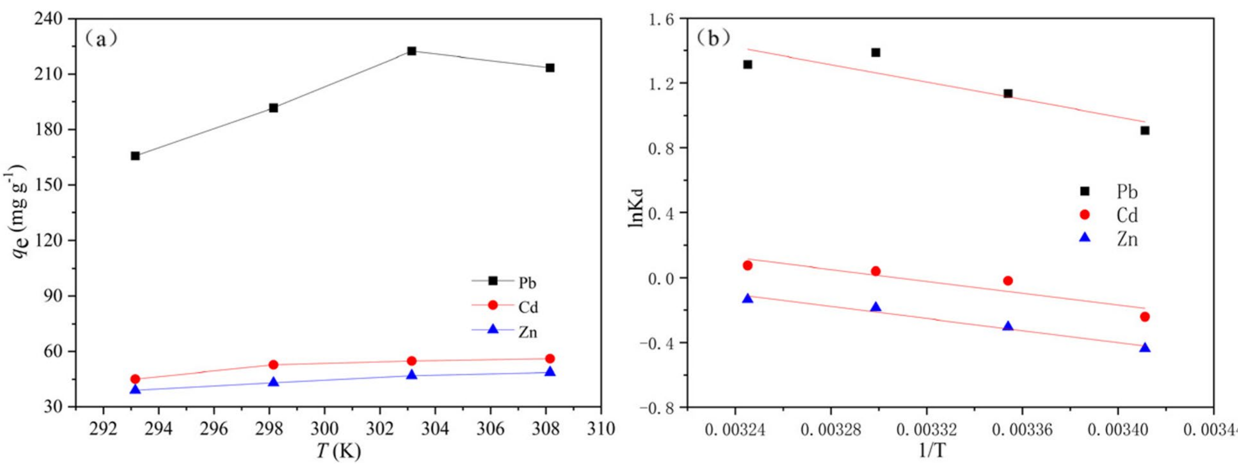

Fig. 8 Effect of temperature (**a**) and the adsorption thermodynamics curve (**b**)

in adsorption capacity [43]. This trend is consistent with findings from other researchers [44]. For Cd^{2+} and Zn^{2+}, increasing the temperature improved their adsorption capacities. However, there was little effect on adsorption quantity when the temperature increased from 30 to 35 °C. Consequently, 30 °C is considered the most suitable temperature for this study.

Equilibrium data obtained at 20, 25, 30 and 35 ℃ were used to calculate the thermodynamic parameters, including ΔG (kJ mol^{-1}), ΔH (kJ mol^{-1}) and ΔS (J (mol K) $^{-1}$). These parameters were determined using the following Eqs. (7), (8), and (9).

$$\Delta G = -NTlnK \tag{7}$$

$$lnK = \frac{\Delta S}{N} - \frac{\Delta H}{NT} \tag{8}$$

$$\Delta G = \Delta H - \mathrm{T}\Delta S \tag{9}$$

In these equations, N [8.314 J (mol K)$^{-1}$], T (K) and K represent the universal gas constant, the adsorption temperature, and the equilibrium constant at temperature T, respectively. The slope and intercept of the curve between ΔG and T were used to determine the values of ΔS and ΔH, as shown in Fig. 8b and Table 4.

The negative ΔG at different experimental temperatures demonstrate that the adsorption process was feasible and spontaneous. The decrease in ΔG with increasing temperature (from 20 to 35 °C) indicates that the adsorption between S12 and heavy metal ions is favored within this temperature range. The positive values of both ΔH and ΔS suggest that the reaction was endothermic and that randomness at the solid/solution interface increased.

Table 4 Thermodynamic result for the adsorption of Pb^{2+}, Cd^{2+} and Zn^{2+} by *A. tumefaciens* S12

Adsorbate	T (°C)	ΔG (kJ·mol^{-1})	ΔH (kJ mol^{-1})	ΔS (J·(mol K) $^{-1}$	r^2
Pb^{2+}	20	-2.21	22	84	0.8027
	25	-2.81			
	30	-3.50			
	35	-3.37			
Cd^{2+}	20	-0.72	24	84	0.9249
	25	-1.31			
	30	-1.83			
	35	-1.93			
Zn^{2+}	20	-0.18	13	44	0.9288
	25	-0.51			
	30	-0.75			
	35	-0.83			

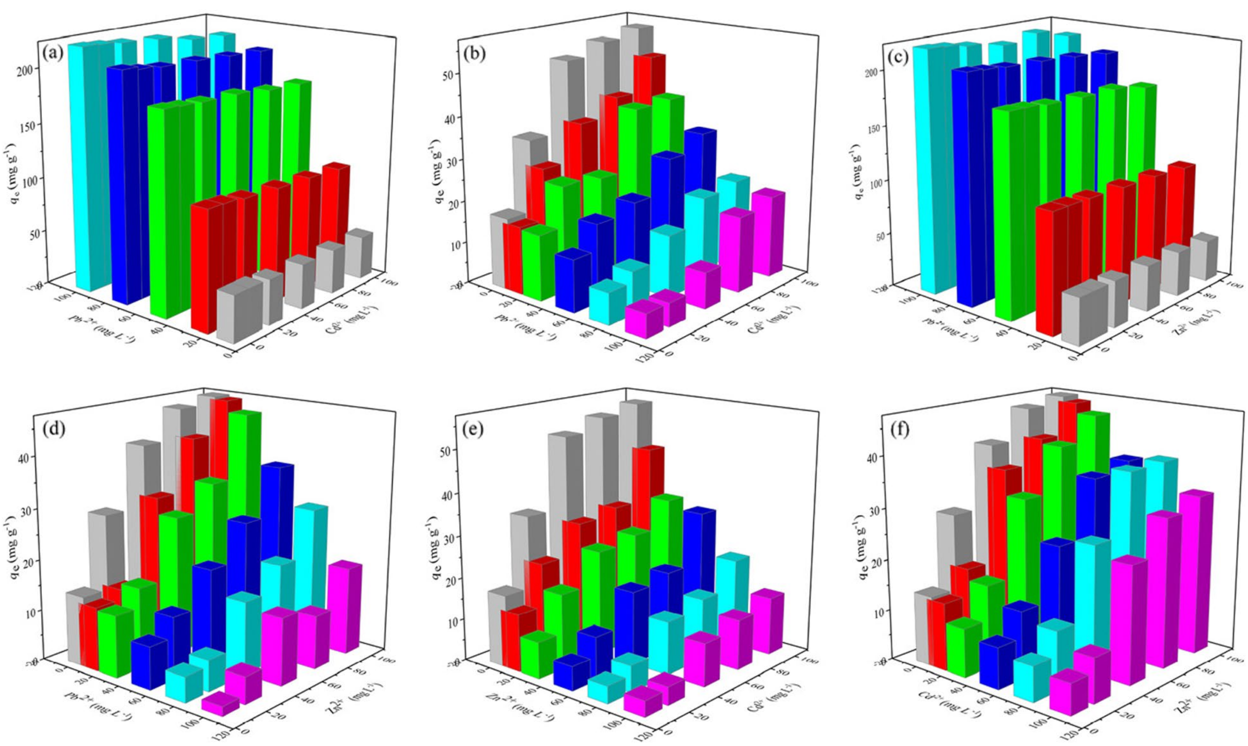

Fig. 9 Adsorption of Pb^{2+}, Cd^{2+} and Zn^{2+} by *A. tumefaciens* S12 in binary metal system ((**a**) and (**b**) are Cd/Pb binary system, (**c**) and (**d**) are Zn/Pb binary system, (**e**) and (**f**) are Zn/Cd binary system)

3.3.6 The adsorption behavior in bimetallic systems

Figure 9 shows the interaction effects between pairs of metal ions. In the Cd/Pb and Zn/Pb binary systems, the presence of Cd^{2+} (Fig. 9a) and Zn^{2+} (Fig. 9c) had negligible effects on the biosorption of Pb^{2+}. The adsorption capacity of Pb^{2+} remained relatively unchanged under varying Pb^{2+} concentrations, even as Cd^{2+} and Zn^{2+} concentrations increased. In contrast, the presence of Pb^{2+} inhibited the ability of *A. tumefaciens* S12 to adsorb Cd^{2+} (Fig. 9b) and Zn^{2+} (Fig. 9d), with increasing Pb^{2+} concentrations leading to a noticeable decrease in the uptake capacity of Cd^{2+} and Zn^{2+}. These findings are consistent with previous research. In the Zn/Cd binary system (Fig. 9e and f), the coexistence of one metal in the solution consistently reduced the removal of the other, indicating that competitive bioadsorption occurred between Cd^{2+} and Zn^{2+} for the available binding sites.

This adsorption behavior may be influenced by the different electronic configurations of the metal elements ([Xe] $4f^{14}5d^{10}6s^26p^2$ for Pb, [Kr] $4d^{10}5s^2$ for Cd, [Ar] $3d^{10}4s^2$ for Zn) [45]. Metals with more orbitals and outer orbital electrons exhibit stronger affinities with functional groups. Additionally, differences in electronegativity and ionic radius contribute to these results. The electronegativity of Pb^{2+}, Cd^{2+} and Zn^{2+} are 2.33, 1.39 and 1.65, respectively, and their ion radii are 1.32, 0.97 and 0.74 Å, respectively [46–48]. Metal ions with higher electronegativity and larger ionic radii are more easily adsorbed by adsorbents.

In bimetallic systems, Pb^{2+} showed a greater affinity for *A. tumefaciens* S12 than Cd^{2+} and Zn^{2+}, based on the physical properties of the metals. This observation is consistent with the constants in Table 2 fitted by the Langmuir model. The above explanations demonstrate that the biosorption of Pb^{2+} ions is preferred over Cd^{2+} and Zn^{2+} in binary systems. For the Cd/Zn binary system, the competitive bioadsorption may be attributed to their similar affinities for the binding sites and the limited number of adsorption sites on the adsorbent.

3.4 Adsorption mechanism

3.4.1 SEM and EDS spectroscopy

The morphological changes in biomass before and after the adsorption of Pb^{2+}, Cd^{2+} and Zn^{2+} can be observed in Fig. 10. The pristine *A. tumefaciens* S12 cells were rod-shaped, with smooth and regular surfaces (Fig. 10a). However, after exposure to heavy metal ions, some *A. tumefaciens* S12 cells showed signs of structural damage,

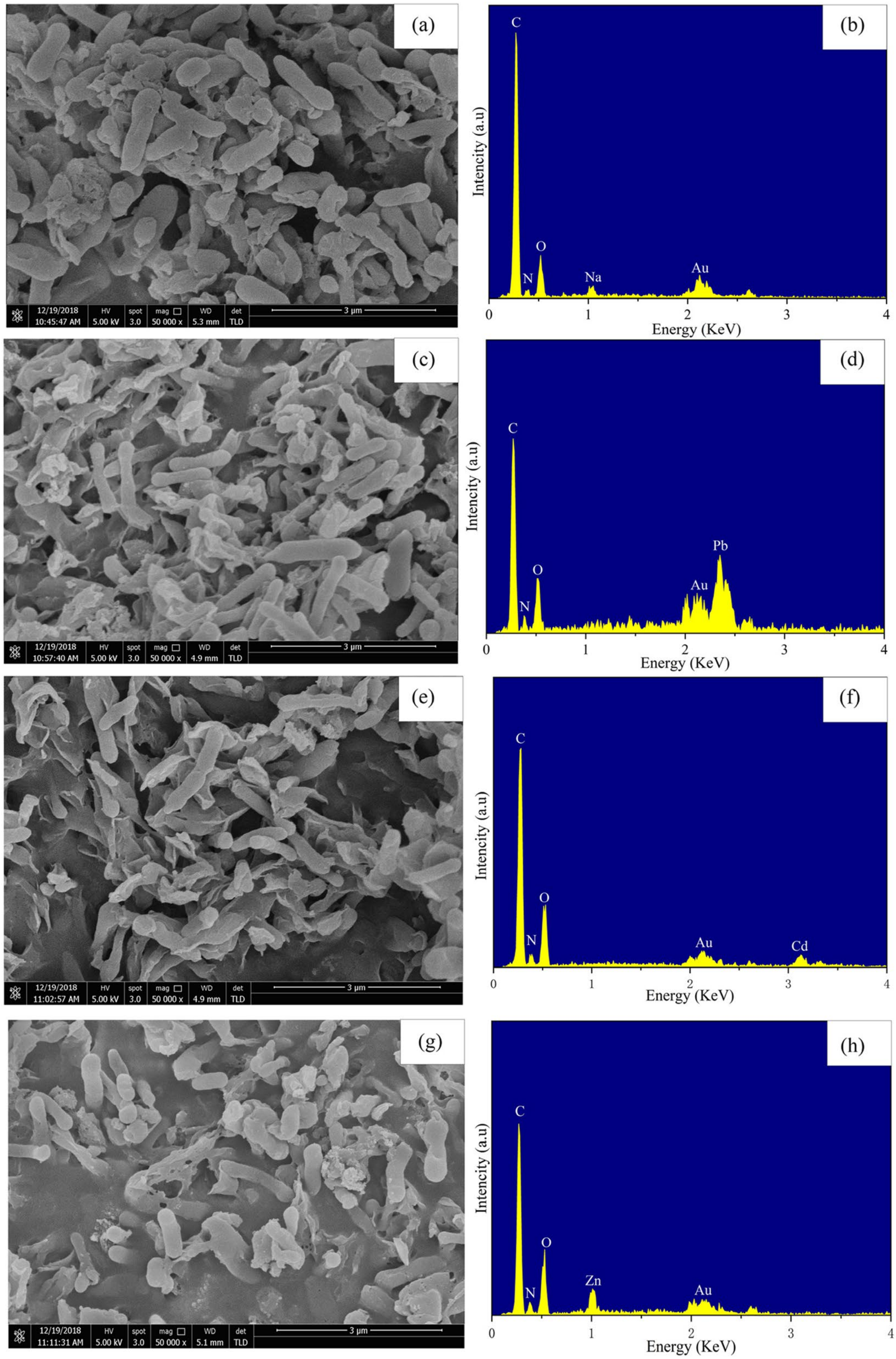

Fig. 10 SEM and EDS results of before (**a** and **b**) and after the adsorption of Pb^{2+} (**c** and **d**), Cd^{2+} (**e** and **f**) and Zn^{2+} (**g** and **h**) by *A. tumefaciens* S12

which may be attributed to the restriction of microbial metabolic activity due to nutrient deficiency and the toxicity of heavy metals. Similar observations were reported by Huang et al. [49]. Additionally, the aggregation of *A. tumefaciens* S12 cells became more pronounced, and their surfaces appeared rougher after the adsorption of Pb^{2+}, Cd^{2+} and Zn^{2+} (Fig. 10c, e and g). This roughness likely resulted from mechanical force damage and interactions between surfactants and metal ions [50].

The EDS analysis revealed significant changes in the elemental composition of *A. tumefaciens* S12 after the adsorption of Pb^{2+}, Cd^{2+} and Zn^{2+} compared to the composition before adsorption (Fig. 10b, d, f and h). Distinct peaks corresponding to Pb, Cd, and Zn were observed in the post-adsorption samples, confirming that *A. tumefaciens* S12 successfully absorbed these metal ions. Besides, the disappearance of the Na peak after adsorption suggests that Na^{+} was released from the cells during the process, indicating that ion exchange was involved in the adsorption mechanism [51].

3.4.2 FTIR analysis

FTIR analysis can be used to identify the functional groups present on the surface of *A. tumefaciens* S12 cells. As shown in Fig. 11a, the surface composition of *A. tumefaciens* S12 is complex, with various functional groups identified through the FTIR spectra. The broad band observed at 3600–3200 cm^{-1} corresponds to overlapping peaks from hydroxyl (-OH) and amine (-NH) groups. In addition, the peaks at 3000–2800 cm^{-1} are attributed to C-H stretching vibrations in alkyl chains [52]. Strong bands at 1655, 1547 and 1239 cm^{-1} are associated with amide bond formation [53, 54]. Similarly, absorption bands around 1453 and 1384 cm^{-1} have been identified as the C-O stretching mode of -COOH groups and C-H stretching vibrations, respectively [49]. Furthermore, the peaks at 1083 and 1049 cm^{-1} indicate the presence of organic phosphate groups [55]. The peaks between 701 and 881 cm^{-1} are mainly due to P-O-C and P-O-P stretching, originating from phospholipids and ribose phosphate chain pyrophosphate [56]. This analysis reveals that hydroxyl, carboxyl, amino, and phosphate groups are present in *A. tumefaciens* S12, with the primary components being polysaccharides, proteins, and phospholipids.

The shifts in peak positions and changes in intensity observed in the FTIR spectra of *A. tumefaciens* S12 with and without heavy metals (Fig. 11b–d) suggest that the functional groups represented by these peaks are involved in the adsorption process. After the adsorption of Pb^{2+}, Cd^{2+} and Zn^{2+}, the peak at 3297 cm^{-1} shifted to 3284, 3295 and 3295 cm^{-1}, respectively, with a corresponding reduction in peak intensity. Similarly, the intensity of the peaks at 2970 and 2927 cm^{-1} decreased after adsorption. Furthermore, both the intensity and position of the adsorption peaks for amide groups changed. Moreover, the peaks at 1083 and 1049 cm^{-1} observed for pristine *A. tumefaciens* S12 cells merged into a single peak and shifted to 1071, 1060 and 1069 cm^{-1} after adsorption. These changes conclusively indicate that multiple functional groups, including hydroxyl, amino, carboxyl,

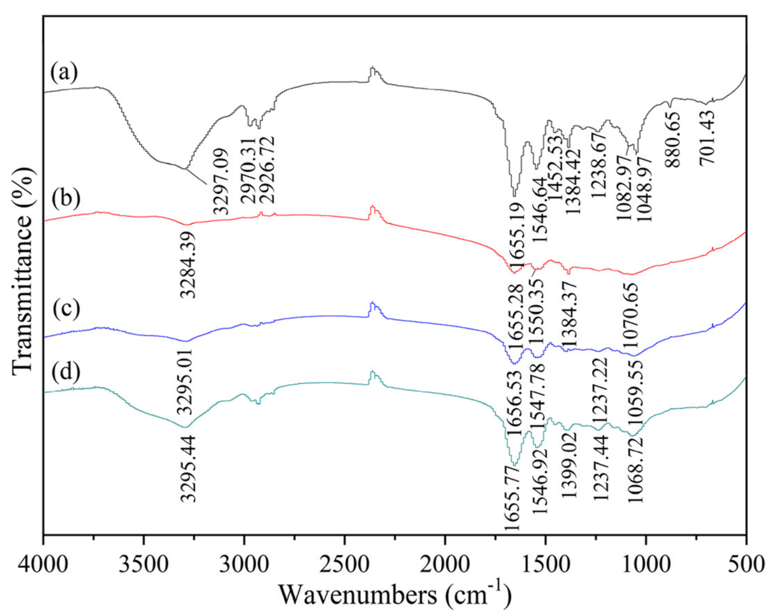

Fig. 11 FTIR spectra of before and after adsorption of Pb^{2+}, Cd^{2+} and Zn^{2+} by *A. tumefaciens* S12 (**a**: before, **b**: Pb^{2+},**c**: Cd^{2+}, **d**: Zn^{2+})

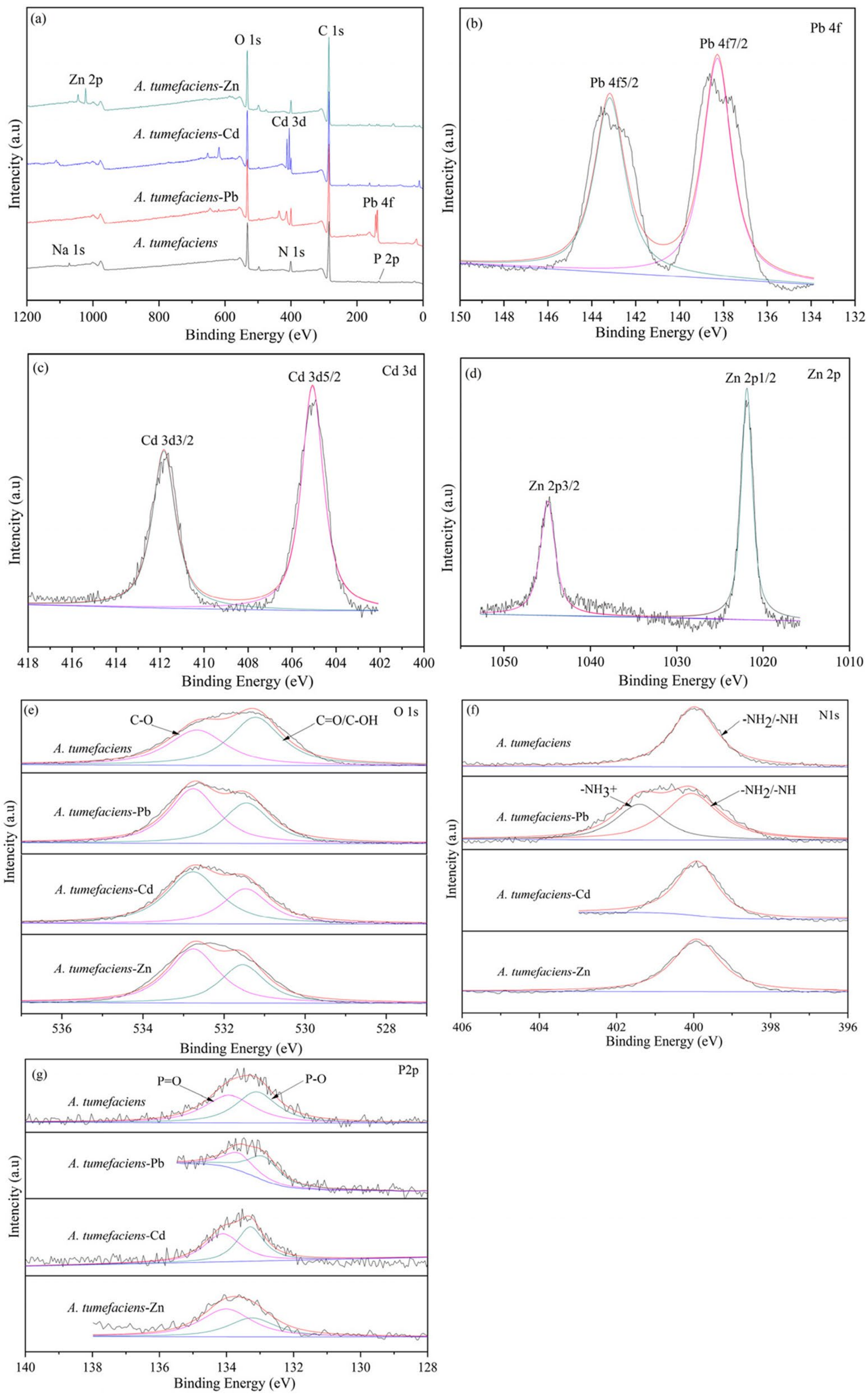

Fig. 12 XPS spectra of *A. tumefaciens* S12 before and after adsorption of Pb^{2+}, Cd^{2+} and Zn^{2+} (**a**: broad scan, **b**: Pb 4f, **c**: Cd, 3d, **d**: Zn 2p,**e**: O 1 s, **f**: N 1 s, **g**: P 2p)

and phosphate, participate in the adsorption process and play a dominant role in the removal of metal ions.

3.4.3 XPS analysis

XPS is a powerful tool for elucidating the adsorption mechanism of *A. tumefaciens* S12 with heavy metal ions, as it provides detailed information on the chemical composition of the samples and chemical-state changes in the elements under study. By comparing the wide-scan results of *A. tumefaciens* S12 before and after adsorption (Fig. 12a), it is clear that Pb 4f, Cd 3d and Zn 2p peaks appear distinctly in the XPS spectra, confirming that *A. tumefaciens* S12 successfully captured these three ions. The spectrum analysis of Pb^{2+}-bound *A. tumefaciens* S12 (Fig. 12b) reveals a characteristic binding energy for Pb^{2+} at 138.3 eV, corresponding to the Pb 4f7/2 peak. Additionally, the presence of a Pb 4f5/2 peak at 143.2 eV suggests that Pb^{2+} was chemisorbed to functional groups on the cell surface [35]. Figure 12c shows that the Cd peak is split into two components, 3d3/2 (411.8 eV) and Cd3d5/2 (405.1 eV). Figure 12d presents the Zn 2p photoelectron spectrum, featuring Zn 2p3/2 and 2p1/2 peaks at 1021.9 and 1044.9 eV, respectively, consistent with literature values [57].

Interestingly, the wide-scan results also reveal a prominent Na 1 s peak in the pristine *A. tumefaciens* S12, which disappears after adsorption of Pb^{2+}, Cd^{2+}, and Zn^{2+}. This suggests that Na^{+} was displaced during the adsorption process, as Pb^{2+}, Cd^{2+}, and Zn^{2+} have a stronger affinity for the functional groups on the biosorbent. This displacement hints at an ion-exchange mechanism being involved in the adsorption process.

Table 5 highlights a noticeable decrease in the proportion of N, O, and P elements in *A. tumefaciens* S12 after adsorption of the heavy metal ions. Figure 12 and Table 6 further show the high-resolution XPS spectra for O 1 s, N 1 s, and P 2p.

Figure 12e shows that the O 1 s peaks in *A. tumefaciens* S12, both before and after metal ion adsorption, consist of C=O/C–OH and C-O groups. Prior to adsorption, the O 1 s spectrum reveals peaks for C=O/C–OH and C-O at 531.2 and 532.7 eV, respectively [58]. Post-adsorption of Pb^{2+}, Cd^{2+}, and Zn^{2+}, the area of the C=O/C–OH peak decreases from 55% to 42, 37, and 38%, respectively, indicating that hydroxyl and carboxyl groups played a significant role in the adsorption process, aligning with FTIR results. Moreover, the binding energies of C=O/C–OH groups shift to 531.5 eV, and the C-O binding energy

Table 5 The composition on the surface of *A. tumefaciens* S12 from XPS spectra

Sample	Surface composition (%)						
	C1s	$N1_S$	O1s	$P2_P$	Pb 4f	Cd 3d	Zn 2p
A.tumefaciens	68.44	8.18	22.38	1	-	-	-
A.tumefaciens-Pb	70.63	7.21	20.62	0.47	1.07	-	-
A.tumefaciens-Cd	71.13	5.6	20.82	0.88	-	1.56	-
A.tumefaciens-Zn	71.17	6.12	20.38	0.64	-	-	1.73

Table 6 The XPS spectra carves fitting results of *A. tumefaciens* S12 before and after adsorption of Pb^{2+}, Cd^{2+} and Zn^{2+}

Element	*A.tumefaciens*		*A.tumefaciens*-Pb		*A.tumefaciens*-Cd		*A.tumefaciens*-Zn	
	Assignment	BE (eV)	Assignment	BE (eV)	Assignment	BE (eV)	Assignment	BE (eV)
O1s	C-O	532.7	C-O	532.8	C-O	532.8	C-O	532.8
	C=O/C–OH	531.2	C=O/C–OH	531.5	C=O/C–OH	531.5	C=O/C–OH	531.5
$N1_S$	$-NH_2$/-NH	400.0	$-NH_2$/-NH	400.1	$-NH_2$/-NH	399.9	$-NH_2$/-NH	399.9
	-	-	$-NH_3^+$	401.4	-	-	-	-
$P2_P$	P-O	133.1	P-O	132.9	P-O	133.3	P-O	133.2
	P=O	133.9	P=O	133.7	P=O	134.1	P=O	134.0
Pb 4f	-	-	Pb 4f 5/2	143.2			-	-
	-	-	Pb 4f 7/2	138.3			-	-
Cd 3d	-	-	-	-	Cd 3d3/2	411.8		
	-	-	-	-	Cd 3d5/2	405.1		
Zn 2p							Zn 2p1/2	1021.9
							Zn 2p3/2	1044.9

changes to 532.8 eV after metal ion binding. This suggests that these functional groups were actively involved in the adsorption process, likely through charge transfer interactions with Pb^{2+}, Cd^{2+}, and Zn^{2+}.

Figure 12f presents the fitted N 1 s spectra. Before the adsorption of Pb^{2+}, Cd^{2+}, and Zn^{2+}, a single N 1 s peak at 400.0 eV, corresponding to -NH_2 or –NH groups from proteins, is observed. After Pb^{2+} adsorption, the complexation reaction between -NH_2 or –NH groups and Pb^{2+} results in the protonation of amines, as evidenced by the emergence of a new weak N 1 s peak at approximately 401.4 eV. The reaction is illustrated by the following equations:

$$R-NH_2 + Pb^{2+} \rightarrow R-NH_2Pb^{2+} \tag{10}$$

$$R-NH + Pb^{2+} \rightarrow R-NHPb^{2+} \tag{11}$$

Additionally, the binding energy of -NH_2 or -NH groups increases to 400.1 eV due to Pb^{2+} sharing lone pair electrons provided by N atoms, which diminishes electron cloud density [59]. For Cd^{2+} and Zn^{2+} adsorption, the binding energies of -NH or -NH_2 groups decrease to 399.9 eV, indicating coordination bonds formed between N atoms and the metal ions. In these bonds, Cd^{2+} and Zn^{2+} share electrons with N atoms, resulting in a decrease in binding energy due to the increased electron cloud density around the N atoms.

Although the atomic contents (%) of P is lower compared to O and N, the change in P content after adsorption is significant, as shown in Table 5. The P2p spectrum of *A. tumefaciens* 12 (Fig. 12g) features two peaks assigned to P-O (133.1 eV) and P=O (133.9 eV) [60, 61]. This confirms that phospholipids, containing phosphate groups with *P*=O and P-O functionalities, are part of the surface composition of *A. tumefaciens* S12. The shifts in their binding energies after adsorption suggest that these phosphate groups were involved in the adsorption process through complexation and electrostatic attraction.

In summary, based on the XPS spectra analysis, *A. tumefaciens* S12 proves to be an excellent adsorbent for Pb^{2+}, Cd^{2+}, and Zn^{2+} because of the abundance of functional groups containing N, O, and P. These groups facilitate the formation of complexes with the heavy metal ions, with mechanisms such as ion exchange, complexation, and electrostatic attraction likely playing a dominant role in the adsorption process.

4 Conclusion and future prospect

A.tumefaciens 12 with heavy metal tolerance isolated from AMD has demonstrated exceptional tolerance to heavy metals, specifically Pb^{2+}, Cd^{2+}, and Zn^{2+}. This bacterium not only exhibits high resistance to these metals with MIC of 400 mg L^{-1} for Pb^{2+}, 300 mg L^{-1} for Cd^{2+}, and 250 mg L^{-1} for Zn^{2+}, but also shows effective adsorption capabilities. The adsorption was obviously impacted by pH, biomass dosage, initial Pb^{2+}, Cd^{2+} and Zn^{2+} concentration and adsorption temperature. The adsorption process is best described by a pseudo-second-order chemisorption model, and the Langmuir isotherm effectively fits the adsorption data for Pb^{2+}, Cd^{2+} and Zn^{2+} with maximum adsorption capacities of 234, 58 and 51 mg g^{-1}, respectively. The adsorption of Pb^{2+}, Cd^{2+} and Zn^{2+} by *A. tumefaciens* 12 was spontaneous and endothermic in nature through thermodynamic study. In bimetallic systems, *A. tumefaciens* 12 showed a preference for adsorbing Pb^{2+} over Cd^{2+} and Zn^{2+}, with competition observed between Cd^{2+} and Zn^{2+} for binding sites. The high adsorption efficiency of *A. tumefaciens* 12 is attributed to the presence of functional groups such as hydroxyl, carboxyl, amino, and phosphate on its surface, which facilitate ion-exchange and complexation with the metal ions. This makes *A. tumefaciens* 12 an excellent candidate for bioremediation, offering an economical and environmentally friendly method for the removal of heavy metals from wastewater.

To enhance the applicability and feasibility of *A. tumefaciens* 12, further research is necessary. Conducting pilot-scale experiments using actual wastewater, such as mining effluents containing heavy metals, would help explore its practical application conditions and feasibility. Additionally, several limitations need to be addressed. For instance, it is crucial to develop effective methods for separating metal-laden cells from water bodies. Furthermore, lacking of specificity for heavy metals, simple biosorbents could be hard to recycle the desired metals.

A. tumefaciens 12 is a novel and promising bacterium for the removal of heavy metals. Further research could provide a more comprehensive understanding of its metal absorption capabilities. Firstly, exploring the bacterium's ability to absorb additional heavy metals, such as Cu^{2+}, Ni^{2+}, and Cr^{6+}, would broaden its potential applications. Delving deeper into the specific mechanisms involved in each process could also offer valuable insights into how the bacterium interacts with heavy metal ions, enabling the optimization of these processes for more efficient biosorption. Additionally, evaluating the long-term effects of biosorption is essential. This includes assessing the potential risks associated with releasing genetically modified bacteria into the environment and understanding the impact of repeated heavy metal exposure on bacterial viability and performance over time. These areas of research are crucial for fully realizing the potential of *A. tumefaciens* 12 in practical applications.

Acknowledgements
The authors wish to thank (Project No. 82260632), Guizhou Science and Technology Plan Project (Qinke Platform talent [2019]-011, [2020]-019 and [2020]-037), Science and Technology Cooperation Support Project of Zunyi (Project No. HZ (2020)72 and HZ (2021)293), and Scientific Research Project (Youth project) of college and university of Guizhou Provincial Department of Education (Project No. Qin Education Technology [2022]243).

Authors' contributions
The manuscript draft was interpreted and written by Shuli Liu. Prof. Yan Li revised the manuscript and provided technical support. Prof. Xiaojun Xu supervised the research. Changhua He provided Software and helped to analyze data. Zhangyang Liu did formal analysis.

Funding
This work was supported by Guizhou Science and Technology Plan Project (Qinke Platform talent [2019]-011, [2020]-019 and [2019]-037), Science and Technology Cooperation Support Project of Zunyi (Project No. HZ (2020)72 and HZ (2021)293), and Scientific Research Project (Youth project) of college and university of Guizhou Provincial Department of Education (Project No. Qin Education Technology [2022]243).

Data availability
All data generated or analyzed during this study are included in this article.

Declarations

Competing interests
The authors declare they have no conflict of interest. The authors declare they have no competing interests.

Received: 14 November 2023 Accepted: 10 October 2024
Published online: 31 October 2024

References
1. Ambade B, Sankar TK, Kumar A, Sethi SS. Characterization of PAHs and n-alkanes in atmospheric aerosol of Jamshedpur city, India. J Hazard Toxic Radioact Waste. 2020;24:04020003.
2. Ambade B. Seasonal variation and sources of heavy metals in hilltop of Dongargarh, Central India. Urban Clim. 2014;9:155–65.
3. Johnson DB, Hallberg KB. Acid mine drainage remediation options: a review. Sci Total Environ. 2005;338:3–14.
4. Park I, Tabelin CB, Jeon S, Li X, Seno K, Ito M, et al. A review of recent strategies for acid mine drainage prevention and mine tailings recycling. Chemosphere. 2019;219:588–606.
5. Masindi V, Fosso-Kankeu E, Mamakoa E, Nkambule TTI, Mamba BB, Naushad M, et al. Emerging remediation potentiality of struvite developed from municipal wastewater for the treatment of acid mine drainage. Environ Res. 2022;210:112944.
6. Anekwe IMS, Isa YM. Bioremediation of acid mine drainage – Review. Alex Eng J. 2023;65:1047–75.
7. Sharma S, Sharma M, Kumar R, Akhtar MS, Umar A, Alkhanjaf AAM, et al. Recent advances and mechanisms of microbial bioremediation of nickel from wastewater. Environ Sci Pollut R. 2024;31:40224–44.
8. Patidar K, Ambade B, Mohammad F, Soleiman AA. Microplastics as heavy metal vectors in the freshwater environment: Distribution, variations, sources and health risk. Phys Chem Earth. 2023;131:103448.
9. Huang H, Jia Q, Jing W, Dahms HU, Wang L. Screening strains for microbial biosorption technology of cadmium. Chemosphere. 2020;251:126428.
10. Ramirez Calderon OA, Abdeldayem OM, Pugazhendhi A, Rene ER. Current updates and perspectives of biosorption technology: an alternative for the removal of heavy metals from wastewater. Curr Pollut Rep. 2020;6:8–27.
11. Diaz A, Marrero J, Cabrera G, Coto O, Gomez JM. Biosorption of nickel, cobalt, zinc and copper ions by Serratia marcescens strain 16 in mono and multimetallic systems. Biodegradation. 2022;33:33–43.
12. Ihsanullah, Abbas A, Al-Amer AM, Laoui T, Al-Marri MJ, Nasser MS, et al. Heavy metal removal from aqueous solution by advanced carbon nanotubes: Critical review of adsorption applications. Sep Purif Technol. 2016;157:141–61.
13. Priya AK, Gnanasekaran L, Dutta K, Rajendran S, Balakrishnan D, Soto-Moscoso M. Biosorption of heavy metals by microorganisms: Evaluation of different underlying mechanisms. Chemosphere. 2022;307:135957.
14. He J, Li Y, Wang C, Zhang K, Lin D, Kong L, et al. Rapid adsorption of Pb, Cu and Cd from aqueous solutions by β-cyclodextrin polymers. Appl Surf Sci. 2017;426:29–39.
15. Bano A, Hussain J, Akbar A, Mehmood K, Anwar M, Hasni MS, et al. Biosorption of heavy metals by obligate halophilic fungi. Chemosphere. 2018;199:218–22.
16. Oliveira RC, Hammer P, Guibal E, Taulemesse JM, Garcia O. Characterization of metal–biomass interactions in the lanthanum(III) biosorption on *Sargassum sp.* using SEM/EDX, FTIR, and XPS: Preliminary studies. Chem Eng J. 2014;239:381–91.
17. Li X, Ming Q, Cai R, Yue T, Yuan Y, Gao Z, et al. Biosorption of Cd^{2+} and Pb^{2+} from apple juice by the magnetic nanoparticles functionalized lactic acid bacteria cells. Food Control. 2020;109:106916.
18. Dusengemungu L, Kasali G, Gwanama C, Ouma KO. Recent advances in biosorption of copper and cobalt by filamentous fungi. Front Microbiol. 2020;11:582016.
19. Ahmad A, Bhat AH, Buang A. Biosorption of transition metals by freely suspended and Ca-alginate immobilised with *Chlorella vulgaris*: Kinetic and equilibrium modeling. J Clean Prod. 2018;171:1361–75.
20. Chen SH, Cheow YL, Ng SL, Ting ASY. Mechanisms for metal removal established via electron microscopy and spectroscopy: a case study on metal tolerant fungi *Penicillium simplicissimum*. J Hazard Mater. 2019;362:394–402.
21. Munoz AJ, Ruiz E, Abriouel H, Galvez A, Ezzouhri L, Lairini K, et al. Heavy metal tolerance of microorganisms isolated from wastewaters: Identification and evaluation of its potential for biosorption. Chem Eng J. 2012;210:325–32.
22. Jakovljevic V, Grujic S, Simicc Z, Ostojic A, Radojevicc I. Finding the best combination of autochthonous microorganisms with the most effective biosorption ability for heavy metals removal from wastewater. Front Microbiol. 2022;13:1017372.
23. Imron MF, Kurniawan SB, Abdullah SRS. Resistance of bacteria isolated from leachate to heavy metals and the removal of Hg by *Pseudomonas aeruginosa* strain FZ-2 at different salinity levels in a batch biosorption system. Sustain Environ Res. 2021;31:14.
24. Teng Z, Shao W, Zhang K, Huo Y, Zhu J, Li M. Pb biosorption by *Leclercia adecarboxylata*: Protective and immobilized mechanisms of extracellular polymeric substances. Chem Eng J. 2019;375:122113.
25. Luo L, LuoY, Qiu P, Jiang D, Huang X. Simultaneous and efficient removal of ammonium and nitrate by a novel isolated *Agrobacterium tumefaciens* M. J Environ Chem Eng. 2023;11:111519.
26. Kumar S, Asif MH, Chakrabarty D, Tripathi RD, Dubey RS, Trivedi PK. Expression of a rice Lambda class of glutathione S-transferase, *OsGSTL2*, in *Arabidopsis* provides tolerance to heavy metal and other abiotic stresses. J Hazard Mater. 2013;248–249:228–37.
27. Chhikara S, Dutta I, Paulose B, Jaiwal PK, Dhankher OP. Development of an *Agrobacterium*-mediated stable transformation method for industrial oilseed crop *Crambe abyssinica* 'BelAnn'. Ind Crop Prod. 2012;37:457–65.
28. Colak F, Atar N, Yazıcıogglu D, Olgun A. Biosorption of lead from aqueous solutions by *Bacillus* strains possessing heavy-metal resistance. Chem Eng J. 2011;173:422–8.
29. Ambade B, Kumar A, Latif M. Characteristics and risk assessment of particulate bound Polycyclic Aromatic Hydrocarbons (PAHs) from traffic sites. Preprint available at Research Square. 2021; https://doi.org/10.21203/rs.3.rs-328364/v1.
30. Limcharoensuk T, Sooksawat N, Sumarnrote A, Awutpet T, Kruatrachue M, Pokethitiyook P, et al. Bioaccumulation and biosorption of Cd^{2+} and Zn^{2+} by bacteria isolated from a zinc mine in Thailand. Ecotox Environ Safe. 2015;122:322–30.
31. Liu T, Hou JH, Wang JB, Wang W, Wang XY, Wu JL. Biosorption of heavy metals from aqueous solution by the novel biosorbent *Pectobacterium* sp. ND2. Environ Prog Sustain. 2018;37:968–74.

32. Abdullah Al-Dhabi N, Arasu MV. Biosorption of hazardous waste from the municipal wastewater by marine algal biomass. Environ Res. 2022;204:112115.
33. Kumar R, Bhatia D, Singh R, Bishnoi NR. Metal tolerance and sequestration of Ni(II), Zn(II) and Cr(VI) ions from simulated and electroplating wastewater in batch process: Kinetics and equilibrium study. Int Biodeter Biodegr. 2012;66:82–90.
34. Luo S, Li X, Chen L, Chen J, Wan Y, Liu C. Layer-by-layer strategy for adsorption capacity fattening of endophytic bacterial biomass for highly effective removal of heavy metals. Chem Eng J. 2014;239:312–21.
35. Manirethan V, Raval K, Rajan R, Thaira H, Balakrishnan RM. Kinetic and thermodynamic studies on the adsorption of heavy metals from aqueous solution by melanin nanopigment obtained from marine source: Pseudomonas stutzeri. J Environ Manage. 2018;214:315–24.
36. Vimalnath S, Subramanian S. Studies on the biosorption of Pb(II) ions using *Pseudomonas putida*. Sep Sci Technol. 2018;53:2550–62.
37. Wang T, Yao J, Yuan Z, Zhao Y, Wang F, Chen H. Isolation of lead-resistant *Arthrobactor* strain GQ-9 and its biosorption mechanism. Environ Sci Pollut R. 2018;25:3527–38.
38. Sayyadi S, Ahmady-Asbchin S, Kamali K, Tavakoli N. Thermodynamic, equilibrium and kinetic studies on biosorption of $Pb^{+}2$ from aqueous solution by *Bacillus pumilus* sp. AS1 isolated from soil at abandoned lead mine. J Taiwan Inst Chem E. 2017;80:701–8.
39. Ozdemir S, Kilinc E, Poli A, Nicolaus B, Güven K. Biosorption of Cd, Cu, Ni, Mn and Zn from aqueous solutions by thermophilic bacteria, *Geobacillus toebii* sub.sp. *decanicus* and *Geobacillus thermoleovorans* sub.sp. *stromboliensis*: Equilibrium, kinetic and thermodynamic studies. Chem Eng J. 2009;152:195–206.
40. Kim SY, Jin MR, Chung CH, Yun YS, Jahng KY, Yu KY. Biosorption of cationic basic dye and cadmium by the novel biosorbent *Bacillus catenulatus* JB-022 strain. J Biosci Bioeng. 2015;119:433–9.
41. Joo JH, Hassan SHA, Oh SE. Comparative study of biosorption of Zn^{2+} by *Pseudomonas aeruginosa* and *Bacillus cereus*. Int Biodeter Biodegr. 2010;64:734–41.
42. Munoz AJ, Espinola F, Ruiz E. Removal of heavy metals by *Klebsiella* sp. 3S1. Kinetics, equilibrium and interaction mechanisms of Zn(II) biosorption. J Chem Technol Biot. 2018;93:1370–80.
43. Khan Z, Nisar MA, Hussain SZ, Arshad MN, Rehman A. Cadmium resistance mechanism in *Escherichia coli* P4 and its potential use to bioremediate environmental cadmium. Appl Microbiol Biot. 2015;99:10745–57.
44. Li X, Xu H, Gao B, Shi X, Sun Y, Wu J. Efficient biosorption of Pb(II) from aqueous solutions by a PAH-degrading strain *Herbaspirillum chlorophenolicum* FA1. J Ind Eng Chem. 2018;57:64–71.
45. Ferreira LS, Rodrigues MS, de Carvalho JCM, Lodi A, Finocchio E, Perego P, et al. Adsorption of Ni^{2+}, Zn^{2+} and Pb^{2+} onto dry biomass of *Arthrospira* (*Spirulina*) *platensis* and *Chlorella vulgaris*. I. Single metal systems. Chem Eng J. 2011;173:326–33.
46. Bayo J. Kinetic studies for Cd(II) biosorption from treated urban effluents by native grapefruit biomass (*Citrus paradisi* L.): The competitive effect of Pb(II), Cu(II) and Ni(II). Chem Eng J. 2012;191:278–87.
47. Rodrigues MS, Ferreira LS, Carvalho JCMd, Lodi A, Finocchio E, Converti A. Metal biosorption onto dry biomass of Arthrospira (Spirulina) platensis and Chlorella vulgaris: Multi-metal systems. J Hazard Mater. 2012;217–218:246–55.
48. Lezcano JM, Gonzalez F, Ballester A, Blazquez ML, Munoz JA, Garcia-Balboa C. Sorption and desorption of Cd, Cu and Pb using biomass from an eutrophized habitat in monometallic and bimetallic systems. J Environ Manage. 2011;92:2666–74.
49. Huang F, Dang Z, Guo CL, Lu GN, Gu RR, Liu HJ, et al. Biosorption of Cd(II) by live and dead cells of *Bacillus cereus* RC-1 isolated from cadmium-contaminated soil. Colloid Surface B. 2013;107:11–8.
50. Ren G, Jin Y, Zhang C, Gu H, Qu J. Characteristics of *Bacillus* sp. PZ-1 and its biosorption to Pb(II). Ecotox Environ Safe. 2015;117:141–8.
51. Manasi, Rajesh V, Santhana Krishna Kumar A, Rajesh N. Biosorption of cadmium using a novel bacterium isolated from an electronic industry effluent. Chem Eng J. 2014;235:176–85.
52. Song W, Liang J, Wen T, Wang X, Hu J, Hayat T, et al. Accumulation of Co(II) and Eu(III) by the mycelia of *Aspergillus niger* isolated from radionuclide-contaminated soils. Chem Eng J. 2016;304:186–93.
53. Wang Y, Yi B, Sun X, Yu L, Wu L, Liu W, et al. Removal and tolerance mechanism of Pb by a filamentous fungus: A case study. Chemosphere. 2019;225:200–8.
54. Saeed A, Iqbal M, Zafar SI. Immobilization of *Trichoderma viride* for enhanced methylene blue biosorption: Batch and column studies. J Hazard Mater. 2009;168:406–15.
55. Khan Z, Rehman A, Hussain SZ. Resistance and uptake of cadmium by yeast, *Pichia hampshirensis* 4Aer, isolated from industrial effluent and its potential use in decontamination of wastewater. Chemosphere. 2016;159:32–43.
56 Du LN, Wang B, Li G, Wang S, Crowley DE, Zhao YH. Biosorption of the metal-complex dye Acid Black 172 by live and heat-treated biomass of *Pseudomonas* sp. strain DY1: Kinetics and sorption mechanisms. J Hazard Mater. 2012;205–206:47–54.
57. Dolic MB, Rajakovic-Ognjanovic VN, Strbac SB, Dimitrijevic SI, Mitric MN, Onjia AE, et al. Natural sorbents modified by divalent Cu^{2+}- and Zn^{2+}-ions and their corresponding antimicrobial activity. New Biotechnol. 2017;39:150–9.
58. Ding P, Song W, Yang Z, Jian J. Influence of Zn(II) stress-induction on component variation and sorption performance of extracellular polymeric substances (EPS) from *Bacillus vallismortis*. Bioproc Biosyst Eng. 2018;41:781–91.
59. Yang F, Liu H, Qu J, Chen JP. Preparation and characterization of chitosan encapsulated *Sargassum* sp. biosorbent for nickel ions sorption. Bioresource Technol. 2011;102:2821–8.
60. Wang K, Liu Q. Adsorption of phosphorylated chitosan on mineral surfaces. Colloid Surface A. 2013;436:656–63.
61. Luo X, Yuan J, Liu Y, Liu C, Zhu X, Dai X, et al. Improved solid-phase synthesis of phosphorylated cellulose microsphere adsorbents for highly effective Pb2+ removal from water: batch and fixed-bed column performance and adsorption mechanism. ACS Sustain Chem Eng. 2017;5:5108–17.

Publisher's Note